Published for SISSA by Springer

Received: March 15, 2018
Revised: July 16, 2018
Accepted: August 20, 2018
Published: August 28, 2018

Measurement of forward top pair production in the dilepton channel in pp collisions at $\sqrt{s} = 13\,\text{TeV}$

The LHCb collaboration

E-mail: stephen.farry@cern.ch

Abstract: Forward top quark pair production is studied in pp collisions in the μeb final state using a data sample corresponding to an integrated luminosity of $1.93\,\text{fb}^{-1}$ collected with the LHCb experiment at a centre-of-mass energy of 13 TeV. The cross-section is measured in a fiducial region where both leptons have a transverse momentum greater than 20 GeV and a pseudorapidity between 2.0 and 4.5. The quadrature sum of the azimuthal separation and the difference in pseudorapidities, denoted ΔR, between the two leptons must be larger than 0.1. The b-jet axis is required to be separated from both leptons by a ΔR of 0.5, and to have a transverse momentum in excess of 20 GeV and a pseudorapidity between 2.2 and 4.2. The cross-section is measured to be

$$\sigma_{t\bar{t}} = 126 \pm 19\,(\text{stat}) \pm 16\,(\text{syst}) \pm 5\,(\text{lumi})\ \text{fb}$$

where the first uncertainty is statistical, the second is systematic, and the third is due to the luminosity determination. The measurement is compatible with the Standard Model prediction.

Keywords: Hadron-Hadron scattering (experiments), Top physics, Heavy quark production, Jet physics, QCD

ArXiv ePrint: 1803.05188

https://doi.org/10.1007/JHEP08(2018)174

JHEP08(2018)174

Contents

1 Introduction 1

2 Detector and simulation 2

3 Event selection and purity 3

4 Cross-section calculation 6

5 Results 9

6 Conclusion 11

The LHCb collaboration 14

JHEP08(2018)174

1 Introduction

The production of top quarks at hadron colliders represents an important test of the Standard Model of particle physics (SM). The top quark is the heaviest known fundamental particle and its production and decay properties are sensitive to a number of scenarios beyond the Standard Model. The unique forward acceptance of the LHCb detector allows measurements in a phase space inaccessible to general purpose detectors such as ATLAS and CMS. Top-quark production in this region receives a higher contribution from quark-antiquark ($q\bar{q}$) annihilation than in the central region and probes higher values of Bjorken-x, where large uncertainties are present in the proton parton distribution functions (PDFs). Precise measurements of top quark production at LHCb can thus be used to constrain PDFs in this region [1]. The greater contribution from quark-initiated production also results in a larger expected charge asymmetry [2, 3] in the forward region than in the central region.

The first observation of top-quark production in the forward region was performed by the LHCb collaboration using data corresponding to an integrated luminosity of $3\,\text{fb}^{-1}$ collected between 2010 and 2012 at centre-of-mass energies of 7 and 8 TeV (Run 1) [4]. The measurement was performed in the μb final state, consisting of a muon and a b-jet, where b-jet refers to a jet originating from the fragmentation of a b quark. A precision of 20% was achieved on the top quark production cross-section. Measurements in this final state have the greatest statistical precision but also suffer from a large background due to the production of a W boson in association with a b-jet. Additionally, this final state does not differentiate between single top quark and top quark pair production. A measurement of top quark production was also performed by the LHCb collaboration in the $\mu b\bar{b}$ and $eb\bar{b}$ final states using the same dataset [5], where the top quark pair ($t\bar{t}$) production cross-section was measured with a precision of 40%. The measurements are in agreement with

the SM prediction, calculated to a precision of 25% to 30% with MCFM [6] using the CT10 PDF set [7], and are limited by uncertainties on the b-tagging efficiency and the background composition.

In 2015 and 2016, a data sample corresponding to an integrated luminosity of $1.93\,\text{fb}^{-1}$ was collected by the LHCb experiment at a centre-of-mass energy of 13 TeV. The increased energy leads to an increase of a factor of ten in the $t\bar{t}$ production cross-section within the LHCb acceptance with respect to collisions at a energy of 8 TeV [8]. The larger cross-section allows access to a number of final states inaccessible in Run 1, including the dilepton final state, where both top quarks decay to a W boson and a b quark, and the W bosons decay leptonically to a lepton and a neutrino. This paper details the first measurement of $t\bar{t}$ production in the μeb final state at LHCb, where the dilepton channel is partially reconstructed by requiring that a muon, an electron and a b-jet are present in the proton-proton (pp) collision, where the leptons are produced by the W boson decay, either directly or through the decay of a tau lepton. This final state yields a high purity with respect to other final states; the selection of two leptons reduces the background from single W-boson production and lepton mis-identification, the choice of different flavour leptons suppresses the contribution from the production of Z bosons, and the b-tagged jet reduces the contribution from light jets.

The LHCb detector is introduced in section 2, the event selection and purity is discussed in section 3, the cross-section calculation is presented in section 4, the results are given in section 5 and the conclusions are drawn in section 6.

2 Detector and simulation

The LHCb detector [9, 10] is a single-arm forward spectrometer covering the pseudorapidity range $2 < \eta < 5$, designed for the study of particles containing b or c quarks. The detector includes a high-precision tracking system consisting of a silicon-strip vertex detector surrounding the pp interaction region, a large-area silicon-strip detector located upstream of a dipole magnet with a bending power of about 4 Tm, and three stations of silicon-strip detectors and straw drift tubes placed downstream of the magnet. The tracking system provides a measurement of momentum, p, of charged particles with a relative uncertainty that varies from 0.5% at low momentum to 1.0% at 200 GeV.[1] The minimum distance of a track to a primary vertex (PV), the impact parameter (IP), is measured with a resolution of $(15 + 29/p_{\text{T}})\,\mu\text{m}$, where p_{T} is the component of the momentum transverse to the beam, in GeV. Photons, electrons and hadrons are identified by a calorimeter system consisting of scintillating-pad and preshower detectors, an electromagnetic calorimeter and a hadronic calorimeter. Muons are identified by a system composed of alternating layers of iron and multiwire proportional chambers. The online event selection is performed by a trigger, which consists of a hardware stage, based on information from the calorimeter and muon systems, followed by a software stage, which applies a full event reconstruction. In this paper, the presence of a muon is used to select candidate events at both stages of

[1] Natural units with $\hbar = c = 1$ are used throughout, so that mass and momentum are measured in units of energy.

JHEP08(2018)174

the trigger; the hardware stage selects muons with a transverse momentum $p_{\mathrm{T}} > 1.76\,\mathrm{GeV}$ and the subsequent software trigger requires that a muon with $p_{\mathrm{T}} > 12\,\mathrm{GeV}$ is present.

To estimate the trigger, reconstruction and selection efficiencies, to determine background contributions, and to compare the selected data sample to theoretical expectations, simulated pp collisions are generated using Pythia8 [11, 12]. The interaction of the generated particles with the detector, and its response, are implemented using the Geant4 toolkit [13] as described in ref. [14].

Results are compared to theoretical predictions calculated at next-to-leading-order (NLO) in perturbative QCD using the POWHEG [15–17], aMC@NLO [18] and MCFM [19, 20] generators. The MCFM prediction is provided at fixed order, while the POWHEG and aMC@NLO predictions are interfaced with Pythia8 to provide a parton shower. In the case of aMC@NLO, the decay of the top quarks is performed using MADSPIN [21, 22]. For background studies, samples of single top quark production in association with a W boson are produced with POWHEG using both the diagram removal and diagram subtraction schemes [23], and samples of WW and WZ boson production are produced using aMC@NLO. For POWHEG and MCFM, the factorisation and normalisation scales are set to the transverse mass of the final state top quarks, while for aMC@NLO, they are set to half the sum of the transverse mass of the final state particles. In all cases, the dynamics of the colliding protons are described by the NNPDF3.0 [24] PDF set, and the mass of the top quark is set to 173 GeV.

3 Event selection and purity

Events containing a high-p_{T} muon and electron of opposite charge in addition to a high-p_{T} jet are selected. Muons are identified as reconstructed tracks that are matched to hits in each of the four muon stations furthest downstream, while electrons are identified as tracks that have left large energy deposits in the preshower detector and electromagnetic calorimeter, in addition to small energy deposits in the hadronic calorimeter. The muons and electrons are required to have p_{T} in excess of 20 GeV, a pseudorapidity in the range $2.0 < \eta < 4.5$, and to be separated by a distance, ΔR, of greater than 0.1 in (η,ϕ) space, where ϕ refers to the azimuthal angle. The reconstructed final state particles used as inputs to the jet building are prepared using a particle flow algorithm and clustered using the anti-k_{T} algorithm as implemented in Fastjet [25], with a distance parameter of 0.5. Requirements are placed on the candidate jet in order to reduce the background formed by particles which are either incorrectly reconstructed or produced in additional pp interactions in the same event. The jet is required to have p_{T} above 20 GeV and a pseudorapidity between 2.2 and 4.2. Separation between the jet and each lepton is ensured by requiring that the ΔR distance between the jet and the leptons is greater than 0.5. A dedicated tagging algorithm is used to select b-jets. The tagger proceeds by building two-body secondary vertices (SVs) using all tracks not associated to any PV in the event, and merging any vertices sharing a common track. A jet is said to be tagged if the event contains an SV with a flight direction satisfying $\Delta R < 0.5$ with respect to the jet axis, where the flight direction is taken to be the vector joining the SV to the primary vertex. More details are given in

JHEP08(2018)174

ref. [26]. Lepton isolation criteria is applied by rejecting events where the transverse component of the vector sum of the momentum of all reconstructed charged particles within $\Delta R < 0.5$ of either lepton is greater than 5 GeV. The leptons are also required to be consistent with originating from a common primary vertex, satisfying IP < 0.04 mm. After applying the full selection, a total of 44 events are retained in the data sample.

In addition to the signal, several physics processes contribute to the selected data sample, either through the presence of an identical final state, or through the misidentification of one or more of the final state objects. The following background processes are considered.

- Lepton misidentification where the muon and electron candidates are produced through the misidentification of one or two hadrons. A number of processes can contribute to this background, including QCD multijet production, W and Z production, and $t\bar{t}$ events where only one lepton is produced in the LHCb acceptance.

- The production of a Z boson in association with a jet contributes either through the $Z \to \tau^+\tau^-$ final state, where the subsequent tau lepton decays produce a final state with a muon and electron, or through the $Z \to \mu^+\mu^-$ and $Z \to e^+e^-$ final states, where one of the final state leptons is misidentified. The associated jet can either be a genuine b-jet produced in association with the Z boson, or due to the misidentification of a charm or light jet.

- The production of a single top quark in association with a W boson, known as $W^\pm t$ production, contributes an identical final state.

- Multiboson processes, such as W^+W^-, $W^\pm Z$ and ZZ production, give rise to a high $p_{\rm T}$ muon and electron in the final state with an associated jet.

As the background from lepton misidentification produces events containing leptons with both same- and opposite-sign charges, the number of background events is determined by first applying the full selection to the data but requiring that the leptons should have the same charge. The b-tagging requirement is also removed to increase the statistical precision. The number of events selected in this same-sign control region is then extrapolated using a factor obtained in an additional background-enriched control sample, where the identification requirements on the electron candidate are reversed. This gives an expectation of 3.5 ± 1.9 events, where the uncertainty is due to the combined statistical uncertainties on the selected number of events and the extrapolation factor, which dominate over any expected systematic effects.

The number of $Z \to \tau^+\tau^-$ events is determined by normalising the number of $Z \to \tau^+\tau^-$ events observed in Pythia8 simulation using the ratio of the number of $Z \to \mu^+\mu^-$ events observed in data and simulation. A total of 0.32 ± 0.03 events are expected, where the uncertainty is obtained by combining the statistical precision of the determination with the uncertainty on the reconstruction and selection efficiency, determined from comparisons between data and simulation. The contributions from misidentification of a lepton in the dimuon and dielectron decay modes of the Z boson are determined using simulation and found to be negligible.

JHEP08(2018)174

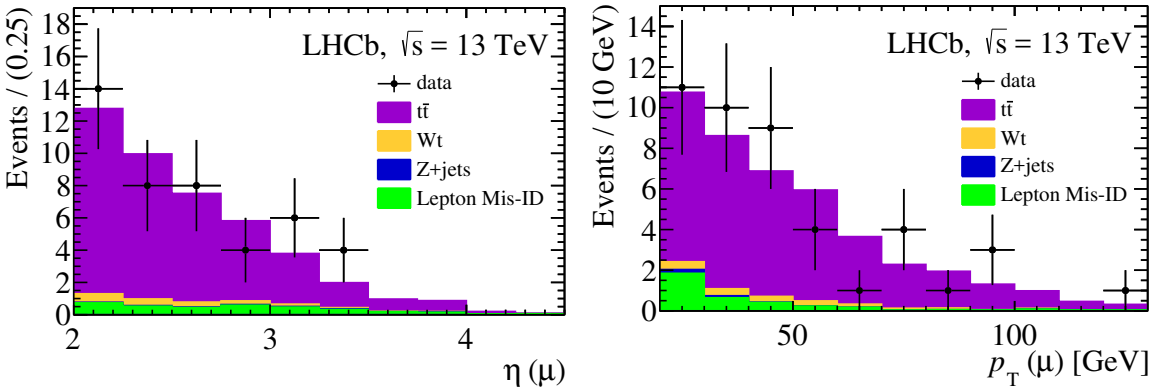

Figure 1. The muon (left) η and (right) p_{T} distribution in data compared to the expected contributions. The $t\bar{t}$ signal yield is determined to be the number of selected events minus the sum of the expected backgrounds. The multiboson background is determined to be negligible.

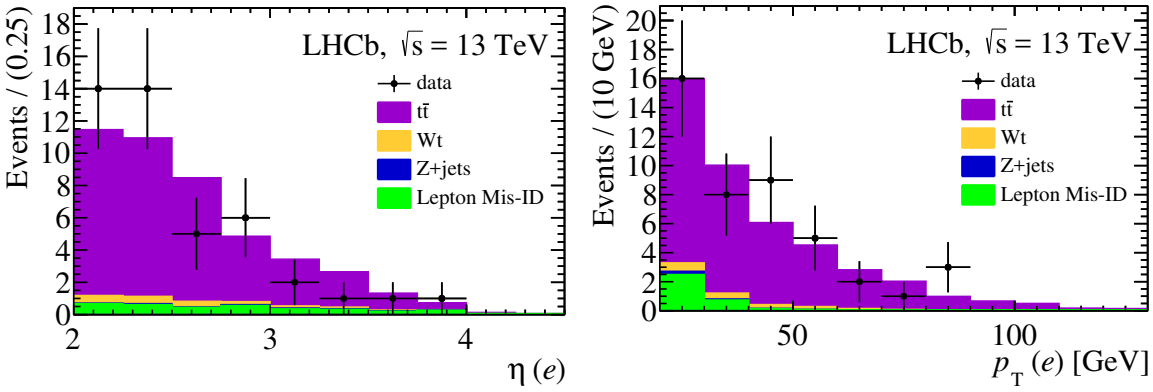

Figure 2. The electron (left) η and (right) p_{T} distribution in data compared to the expected contributions. The $t\bar{t}$ signal yield is determined to be the number of selected events minus the sum of the expected backgrounds. The multiboson background is determined to be negligible.

The $W^{\pm}t$ background is determined using predictions from POWHEG calculated in the diagram removal scheme. The predicted number of events is scaled by the efficiency obtained by reweighting the simulated $t\bar{t}$ sample to match the kinematics of the $W^{\pm}t$ process, yielding an expectation of 1.8 ± 0.5 events. The uncertainty is determined by combining the theoretical uncertainties, determined as described in section 5, with the difference in the cross-section as calculated using the diagram removal and diagram subtraction schemes. An additional systematic uncertainty is added to account for the differences in the reconstruction and selection efficiency. The contribution from multiboson processes is determined from simulations to be negligible.

The total number of expected background events from all sources is 5.6 ± 2.0. The total number of selected events is shown as a function of the muon, electron and jet η and p_{T} distributions in figures 1, 2 and 3. The invariant mass of the muon, electron and jet is shown in figure 4. The expected signal and background contributions are shown, where the signal yield is taken to be the total number of selected events minus the expected

JHEP08(2018)174

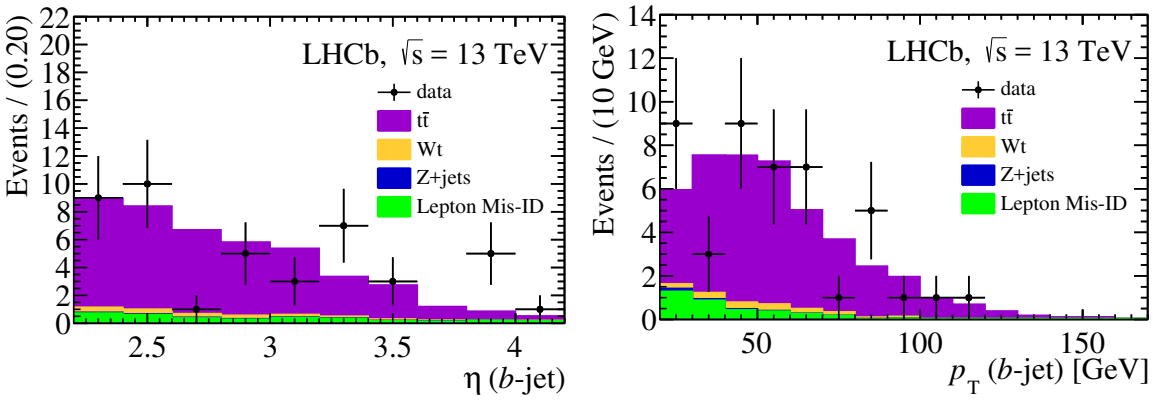

Figure 3. The b-jet (left) η and (right) p_{T} distribution in data compared to the expected contributions. The $t\bar{t}$ signal yield is determined to be the number of selected events minus the sum of the expected backgrounds. The multiboson background is determined to be negligible.

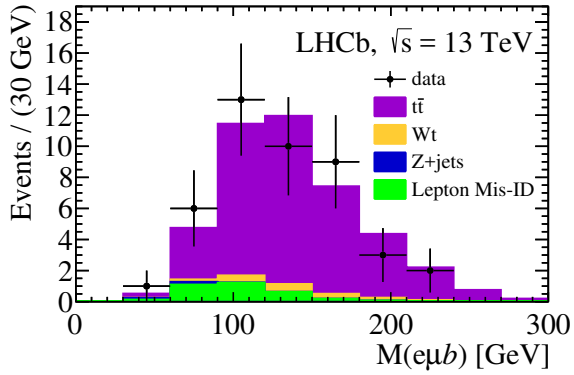

Figure 4. The combined invariant mass of the muon, electron and b-jet in data compared to the expected contributions. The $t\bar{t}$ signal yield is determined to be the number of selected events minus the sum of the expected backgrounds. The multiboson background is determined to be negligible.

background contribution. The lepton misidentification background shape is obtained from the control samples with the electron identification requirements reversed, while all other distributions come from simulation. A reasonable agreement is observed in all distributions.

4 Cross-section calculation

The cross-section, $\sigma_{t\bar{t}}$, is measured in the fiducial region defined by the p_{T}, η, and ΔR requirements placed on the muon, electron and b-jet candidates, and is calculated using the formula

$$\sigma_{t\bar{t}} = \frac{N - N_{\mathrm{bkg}}}{\mathcal{L} \cdot \varepsilon} \cdot \mathcal{F}_{\mathrm{res}}, \tag{4.1}$$

where N is the total number of candidates selected in data, N_{bkg} is the sum of the expected background contributions, $\mathcal{F}_{\mathrm{res}}$ is a resolution factor that accounts for migrations in to and out of the fiducial region, ε is the efficiency to reconstruct and select the signal events, and $\mathcal{L}$ is the integrated luminosity of the data sample.

JHEP08(2018)174

The instantaneous luminosity is measured continuously during the acquisition of physics data by recording the rates of several selected reference processes. The cross-section of these processes is measured during a dedicated data-taking calibration period, using a beam-gas imaging method specific to the LHCb detector [27, 28], which gives a luminosity calibration with an uncertainty of 3.9%. The integrated luminosity of the data sample used, $\mathcal{L}$, is obtained from the accumulated counts of the calibrated rates and is determined to be $1.93 \pm 0.07\,\text{fb}^{-1}$.

The event reconstruction and selection efficiency, ε, can be further divided into eight components

$$\varepsilon = \varepsilon_{\mu}^{\text{rec}} \cdot \varepsilon_{\mu}^{\text{id}} \cdot \varepsilon^{\text{trg}} \cdot \varepsilon_{e}^{\text{rec}} \cdot \varepsilon_{e}^{\text{id}} \cdot \varepsilon^{\text{jet}} \cdot \varepsilon^{\text{tag}} \cdot \varepsilon^{\text{sel}} \tag{4.2}$$

where the equation is ordered from left to right such that, for each component, the efficiency is evaluated for candidates passing the stages to the left. The efficiencies to reconstruct and identify the muon candidate are given by $\varepsilon_{\mu}^{\text{rec}}$ and $\varepsilon_{\mu}^{\text{id}}$ respectively, while ε^{trg} refers to the efficiency to trigger the event on the muon candidate. The efficiencies to reconstruct and identify the electron candidate are given by $\varepsilon_{e}^{\text{rec}}$ and $\varepsilon_{e}^{\text{id}}$ respectively. The efficiency to reconstruct and tag the jet are given by ε^{jet} and ε^{tag} respectively, and the efficiency of the additional selection requirements is given by ε^{sel}.

The efficiencies to reconstruct, identify, and trigger the muon candidate are determined from simulation, where the simulated Pythia8 sample is weighted in the muon p_{T} and η to match NLO predictions from aMC@NLO. Additionally, corrections are applied as a function of the muon p_{T} and η to account for observed differences in the efficiency between data and simulation. The corrections are obtained using a tag-and-probe method on $Z \to \mu^+\mu^-$ events, where one of the muons, the tag, is required to have triggered the event and be fully reconstructed and identified, and a probe is selected that represents the other muon and acts as an unbiased estimator of the efficiency, using similar techniques as those used in ref. [29]. In the case of the reconstruction efficiency, the probe is a track reconstructed using the muon stations and information from tracking detectors not used in the primary track reconstruction algorithms. For the identification efficiency, the probe is a fully reconstructed particle with no identification requirements applied, and for the trigger efficiency, it is a fully reconstructed and identified muon. The uncertainty is determined by combining the statistical uncertainty due to the size of the simulated sample, the uncertainties on the correction factors, and the difference between the efficiencies obtained with and without the NLO weighting.

The efficiencies related to the reconstruction and identification of the electron are again obtained from Pythia8 simulation, weighted as a function of the electron p_{T} and η to match NLO predictions from aMC@NLO. Data-driven studies of these efficiencies are made again using similar techniques to ref. [29]. Corrections to the electron identification efficiency are obtained using a tag-and-probe method on recorded $Z \to e^+e^-$ decays, where the probe is a reconstructed particle with no identification requirements applied. For the electron reconstruction efficiency, no corrections are applied to the simulated sample, but a systematic uncertainty related to the potential mismodelling in simulation is determined by comparing the ratio of the number of $Z \to e^+e^-$ events where either the two electrons

JHEP08(2018)174

are fully reconstructed, or where one of the electrons is only reconstructed as a deposit in the electromagnetic calorimeter. The statistical uncertainty due to the limited size of the simulated sample is combined with the uncertainty on the corrections and the difference in the efficiency before and after weighting to determine the total uncertainty.

The jet reconstruction and tagging efficiencies are determined directly from Pythia8 simulation with NLO weighting in the jet p_{T} and η. A systematic uncertainty on the reconstruction efficiency is determined by comparing the variation in the yield of $Z \to \mu^+\mu^-$ events containing a jet in data and simulation when the quality requirements on the jet are varied, and taking the difference as the uncertainty. The jet tagging efficiency was previously determined to be modelled accurately in simulation to a level of 10% using data collected in Run 1 [26]. The level of agreement is evaluated in the data sample used in this paper by comparing the tagging efficiency of jets containing fully reconstructed $B^{\pm} \to J/\psi K^{\pm}$ decays in data and simulation, where the J/ψ meson is reconstructed through its decay to a muon pair. The signal yield is determined by a fit to the invariant mass of the reconstructed B hadron before and after the tagging requirement is applied. A similar level of agreement between data and simulation is observed as in the previous studies, and consequently the same uncertainty is applied.

The selection efficiency refers to the efficiency of the isolation and impact parameter requirements applied to the leptons. The impact parameter efficiency is obtained from Pythia8 simulation where the impact parameter distribution is smeared using factors obtained from a comparison of $Z \to \mu^+\mu^-$ events in data and simulation. The difference between the efficiency obtained before and after the smearing procedure is taken as a systematic uncertainty. The efficiency of the isolation requirement is obtained directly from Pythia8 simulation, with a systematic uncertainty applied to account for differences in data and simulation. The difference in the efficiency of the requirement when applied to $Z \to \mu^+\mu^-$ events in data and simulation is taken as a systematic uncertainty to account for differences due to the underlying event and contributions from additional pp interactions. An additional contribution to the systematic uncertainty, due to possible mismodelling of the $t\bar{t}$ process, is determined as the maximum difference in the efficiency in simulated $t\bar{t}$ events with different jet multiplicities. A summary of the efficiencies and their uncertainties is given in table 1.

The largest contribution to $\mathcal{F}_{\mathrm{res}}$ arises from the momentum resolution of the electron due to bremsstrahlung. A scaling factor is applied to the electron momentum obtained in simulation to better match the p_{T} spectrum of electrons in $Z \to e^+e^-$ events in data. As the jet resolution also contributes, the level of agreement between data and simulation is evaluated by selecting events containing a Z boson and a jet which are azimuthally opposed. As the ratio of the p_{T} of the jet and the Z boson in these events is expected to be close to unity, the width of the distribution gives an estimate of the jet resolution. Corrections are obtained that are used to smear the reconstructed jet energy in simulation. The resolution factor is determined from simulation with both of these corrections applied, and the difference between the computed values before and after the corrections taken as a systematic uncertainty. The resolution factor is determined to be 1.207 ± 0.006.

JHEP08(2018)174

Source	Efficiency
trigger	0.811 ± 0.016
muon reconstruction	0.930 ± 0.010
electron reconstruction	0.916 ± 0.026
muon identification	0.978 ± 0.008
electron identification	0.918 ± 0.012
jet reconstruction	0.975 ± 0.016
event selection	0.564 ± 0.023
jet tagging	0.556 ± 0.056
total	0.190 ± 0.022

Table 1. The efficiency to fully reconstruct and identify the candidates.

5 Results

Using the formula and inputs described in the previous sections, the cross-section in the fiducial region defined by the p_{T}, pseudorapidity, and ΔR requirements placed on the leptons and the b-jet is determined to be

$$\sigma_{t\bar{t}} = 126 \pm 19\,(\mathrm{stat}) \pm 16\,(\mathrm{syst}) \pm 5\,(\mathrm{lumi})\ \mathrm{fb}$$

where the first uncertainty is statistical, the second is systematic, and the third is due to the luminosity determination. This cross-section is compared to the theoretical predictions obtained from aMC@NLO, POWHEG and MCFM. Three different sources of uncertainty are considered on the theoretical predictions: uncertainties due to the description of the PDFs (δ_{PDF}), the uncertainty due to the choice of renormalisation and factorisation scales (δ_{scale}), and the uncertainty on the value of the strong coupling constant used in the calculation (δ_{α_s}). The uncertainty due to the choice of the top quark mass is expected to be small and is not considered further. The total theoretical uncertainty, δ_{theory}, is determined by combining the individual uncertainties according to the formula $\delta_{\mathrm{theory}} = \sqrt{\delta^2_{\mathrm{PDF}} + \delta^2_{\alpha_s}} + \delta_{\mathrm{scale}}$ [30]. A comparison of the measured cross-section with the predictions is shown in figure 5. The result is shown in the case where the fiducial requirements are placed on the final state muon, electron and b-jet, and where the fiducial requirements are placed on the top quarks, where the top quarks are defined at parton level after QCD radiation. The latter fiducial region requires that both top quarks have a rapidity between 2.0 and 5.0. The measured cross-section in the top quark fiducial region is obtained by extrapolating from the measured fiducial region using predictions from aMC@NLO, which contributes an additional 1.5% uncertainty to the measurement uncertainty, evaluated using the same techniques as for the theoretical predictions described earlier. The cross-section in the top quark fiducial region is additionally compared to predictions from MCFM. The measured cross-section in both fiducial regions is seen to be in agreement with the predictions. A summary of the systematic uncertainties contributing to the measurement is given in table 2. The dominant systematic uncertainty is due to the knowledge of the jet tagging efficiency.

JHEP08(2018)174

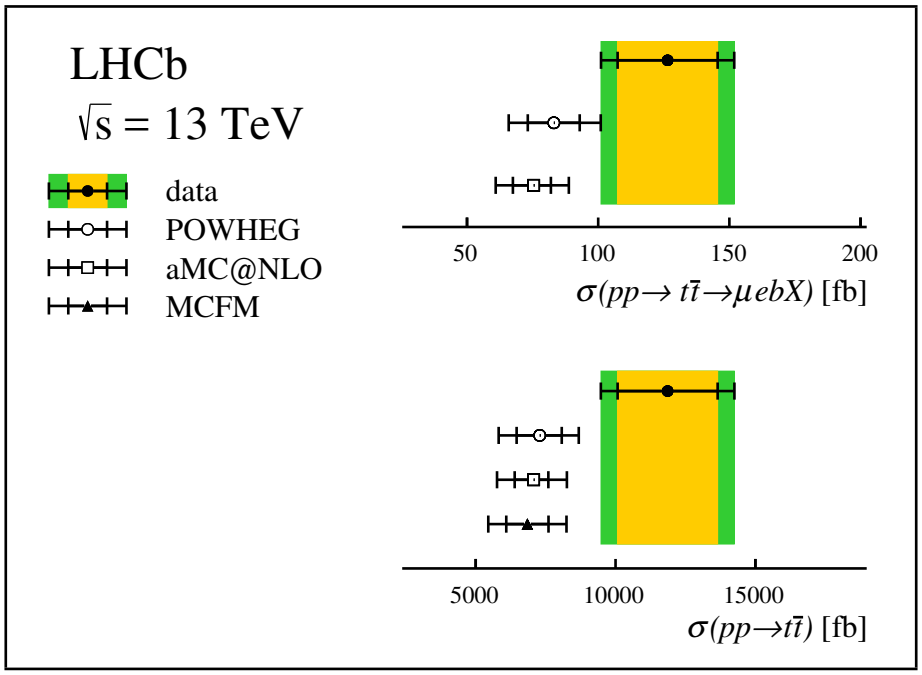

Figure 5. Graphical comparison of the measured cross-sections with the predictions from the aMC@NLO, POWHEG and MCFM generators. For the data, the inner error band represents the statistical uncertainty, and the outer the total, while for the theoretical predictions, the inner band represents the scale uncertainty and the outer represents the total. The prediction is shown (above) for the muon, electron and jet fiducial, and (below) for the top quark fiducial region.

Source	%
trigger	2.0
muon reconstruction	1.1
electron reconstruction	2.8
muon identification	0.8
electron identification	1.3
jet reconstruction	1.6
event selection	4.0
jet tagging	10.0
background	5.1
resolution factor	0.5
total	12.7

Table 2. Summary of the systematic uncertainties on the measurement of the $t\bar{t}$ cross-section in the fiducial region defined by the requirements placed on the leptons and the b-jet, expressed as a percentage of the measured cross-section. An additional uncertainty due to $t\bar{t}$ modelling is considered when extrapolating to the top quark fiducial region.

JHEP08(2018)174

6 Conclusion

The cross-section for top quark pair production in the forward region at LHCb has been measured using the μeb final state, where the presence of a muon, electron and b-jet are used to identify $t\bar{t}$ candidates. The cross-section is measured in two fiducial regions: where fiducial requirements are placed on the final state objects, and where fiducial requirements are placed on the top quarks themselves. The latter fiducial cross-section is obtained by scaling the former by an extrapolation factor obtained from aMC@NLO. The measurement precision of 20% is comparable to prior measurements of top quark production at LHCb in Run 1 and to the precision of the theoretical predictions. The measurement uncertainty is dominated by the statistical precision of the data sample and the knowledge of the b-tagging efficiency.

The final state presented here is selected with a high purity with respect to measurements in other final states. While a number of systematic uncertainties contributing to the measurement are uncorrelated with measurements in other final states, future reductions of the uncertainty on the b-tagging efficiency, common to all final states, will be required in order to fully exploit their complementarity. With the increase in the data-taking capabilities of the LHCb detector in future upgrades [31, 32], measurements in the μeb final state will no longer be statistically limited, and have the potential to achieve the highest precision on the measurement of the $t\bar{t}$ production cross-section at LHCb.

Acknowledgments

We express our gratitude to our colleagues in the CERN accelerator departments for the excellent performance of the LHC. We thank the technical and administrative staff at the LHCb institutes. We acknowledge support from CERN and from the national agencies: CAPES, CNPq, FAPERJ and FINEP (Brazil); MOST and NSFC (China); CNRS/IN2P3 (France); BMBF, DFG and MPG (Germany); INFN (Italy); NWO (The Netherlands); MNiSW and NCN (Poland); MEN/IFA (Romania); MinES and FASO (Russia); MinECo (Spain); SNSF and SER (Switzerland); NASU (Ukraine); STFC (United Kingdom); NSF (U.S.A.). We acknowledge the computing resources that are provided by CERN, IN2P3 (France), KIT and DESY (Germany), INFN (Italy), SURF (The Netherlands), PIC (Spain), GridPP (United Kingdom), RRCKI and Yandex LLC (Russia), CSCS (Switzerland), IFIN-HH (Romania), CBPF (Brazil), PL-GRID (Poland) and OSC (U.S.A.). We are indebted to the communities behind the multiple open-source software packages on which we depend. Individual groups or members have received support from AvH Foundation (Germany), EPLANET, Marie Skłodowska-Curie Actions and ERC (European Union), ANR, Labex P2IO and OCEVU, and Région Auvergne-Rhône-Alpes (France), RFBR, RSF and Yandex LLC (Russia), GVA, XuntaGal and GENCAT (Spain), Herchel Smith Fund, the Royal Society, the English-Speaking Union and the Leverhulme Trust (United Kingdom).

JHEP08(2018)174

References

[1] R. Gauld, *Feasibility of top quark measurements at LHCb and constraints on the large-x gluon PDF*, *JHEP* **02** (2014) 126 [arXiv:1311.1810] [INSPIRE].

[2] A.L. Kagan, J.F. Kamenik, G. Perez and S. Stone, *Top LHCb Physics*, *Phys. Rev. Lett.* **107** (2011) 082003 [arXiv:1103.3747] [INSPIRE].

[3] R. Gauld, *Leptonic top-quark asymmetry predictions at LHCb*, *Phys. Rev.* **D 91** (2015) 054029 [arXiv:1409.8631] [INSPIRE].

[4] LHCb collaboration, *First observation of top quark production in the forward region*, *Phys. Rev. Lett.* **115** (2015) 112001 [arXiv:1506.00903] [INSPIRE].

[5] LHCb collaboration, *Measurement of forward $t\bar{t}$, $W + b\bar{b}$ and $W + c\bar{c}$ production in pp collisions at $\sqrt{s} = 8$ TeV*, *Phys. Lett.* **B 767** (2017) 110 [arXiv:1610.08142] [INSPIRE].

[6] J.M. Campbell and R.K. Ellis, *Radiative corrections to $Zb\bar{b}$ production*, *Phys. Rev.* **D 62** (2000) 114012 [hep-ph/0006304] [INSPIRE].

[7] H.-L. Lai et al., *New parton distributions for collider physics*, *Phys. Rev.* **D 82** (2010) 074024 [arXiv:1007.2241] [INSPIRE].

[8] R. Gauld, *Measuring top quark production asymmetries at LHCb*, LHCb-PUB-2013-009.

[9] LHCb collaboration, *The LHCb Detector at the LHC*, 2008 *JINST* **3** S08005 [INSPIRE].

[10] LHCb collaboration, *LHCb Detector Performance*, *Int. J. Mod. Phys.* **A 30** (2015) 1530022 [arXiv:1412.6352] [INSPIRE].

[11] T. Sjöstrand, S. Mrenna and P.Z. Skands, *A Brief Introduction to PYTHIA 8.1*, *Comput. Phys. Commun.* **178** (2008) 852 [arXiv:0710.3820] [INSPIRE].

[12] T. Sjöstrand, S. Mrenna and P.Z. Skands, *PYTHIA 6.4 Physics and Manual*, *JHEP* **05** (2006) 026 [hep-ph/0603175] [INSPIRE].

[13] GEANT4 collaboration, J. Allison et al., *Geant4 developments and applications*, *IEEE Trans. Nucl. Sci.* **53** (2006) 270 [INSPIRE].

[14] M. Clemencic et al., *The LHCb simulation application, Gauss: Design, evolution and experience*, *J. Phys. Conf. Ser.* **331** (2011) 032023 [INSPIRE].

[15] P. Nason, *A New method for combining NLO QCD with shower Monte Carlo algorithms*, *JHEP* **11** (2004) 040 [hep-ph/0409146] [INSPIRE].

[16] S. Frixione, P. Nason and C. Oleari, *Matching NLO QCD computations with Parton Shower simulations: the POWHEG method*, *JHEP* **11** (2007) 070 [arXiv:0709.2092] [INSPIRE].

[17] S. Alioli, P. Nason, C. Oleari and E. Re, *A general framework for implementing NLO calculations in shower Monte Carlo programs: the POWHEG BOX*, *JHEP* **06** (2010) 043 [arXiv:1002.2581] [INSPIRE].

[18] J. Alwall et al., *The automated computation of tree-level and next-to-leading order differential cross sections and their matching to parton shower simulations*, *JHEP* **07** (2014) 079 [arXiv:1405.0301] [INSPIRE].

JHEP08(2018)174

[19] J.M. Campbell and R.K. Ellis, *An update on vector boson pair production at hadron colliders*, *Phys. Rev.* **D 60** (1999) 113006 [hep-ph/9905386] [INSPIRE].

[20] J.M. Campbell, R.K. Ellis and C. Williams, *Vector boson pair production at the LHC*, *JHEP* **07** (2011) 018 [arXiv:1105.0020] [INSPIRE].

[21] S. Frixione, E. Laenen, P. Motylinski and B.R. Webber, *Angular correlations of lepton pairs from vector boson and top quark decays in Monte Carlo simulations*, *JHEP* **04** (2007) 081 [hep-ph/0702198] [INSPIRE].

[22] P. Artoisenet, R. Frederix, O. Mattelaer and R. Rietkerk, *Automatic spin-entangled decays of heavy resonances in Monte Carlo simulations*, *JHEP* **03** (2013) 015 [arXiv:1212.3460] [INSPIRE].

[23] E. Re, *Single-top Wt-channel production matched with parton showers using the POWHEG method*, *Eur. Phys. J.* **C 71** (2011) 1547 [arXiv:1009.2450] [INSPIRE].

[24] NNPDF collaboration, R.D. Ball et al., *Parton distributions for the LHC Run II*, *JHEP* **04** (2015) 040 [arXiv:1410.8849] [INSPIRE].

[25] M. Cacciari, G.P. Salam and G. Soyez, *FastJet User Manual*, *Eur. Phys. J.* **C 72** (2012) 1896 [arXiv:1111.6097] [INSPIRE].

[26] LHCb collaboration, *Identification of beauty and charm quark jets at LHCb*, 2015 *JINST* **10** P06013 [arXiv:1504.07670] [INSPIRE].

[27] M. Ferro-Luzzi, *Proposal for an absolute luminosity determination in colliding beam experiments using vertex detection of beam-gas interactions*, *Nucl. Instrum. Meth.* **A 553** (2005) 388 [INSPIRE].

[28] LHCb collaboration, *Precision luminosity measurements at LHCb*, 2014 *JINST* **9** P12005 [arXiv:1410.0149] [INSPIRE].

[29] LHCb collaboration, *Measurement of the forward Z boson production cross-section in pp collisions at* $\sqrt{s} = 13$ *TeV*, *JHEP* **09** (2016) 136 [arXiv:1607.06495] [INSPIRE].

[30] LHC Higgs Cross Section Working Group, S. Dittmaier et al., *Handbook of LHC Higgs Cross Sections: 1. Inclusive Observables*, arXiv:1101.0593 [INSPIRE].

[31] LHCb collaboration, *Framework TDR for the LHCb Upgrade: Technical Design Report*, CERN-LHCC-2012-007.

[32] LHCb collaboration, *Expression of Interest for a Phase-II LHCb Upgrade: Opportunities in flavour physics and beyond, in the HL-LHC era*, CERN-LHCC-2017-003.

JHEP08(2018)174

The LHCb collaboration

R. Aaij[40], B. Adeva[39], M. Adinolfi[48], Z. Ajaltouni[5], S. Akar[59], J. Albrecht[10], F. Alessio[40], M. Alexander[53], A. Alfonso Albero[38], S. Ali[43], G. Alkhazov[31], P. Alvarez Cartelle[55], A.A. Alves Jr[59], S. Amato[2], S. Amerio[23], Y. Amhis[7], L. An[3], L. Anderlini[18], G. Andreassi[41], M. Andreotti[17,g], J.E. Andrews[60], R.B. Appleby[56], F. Archilli[43], P. d'Argent[12], J. Arnau Romeu[6], A. Artamonov[37], M. Artuso[61], E. Aslanides[6], M. Atzeni[42], G. Auriemma[26], I. Babuschkin[56], S. Bachmann[12], J.J. Back[50], A. Badalov[38,m], C. Baesso[62], S. Baker[55], V. Balagura[7,b], W. Baldini[17], A. Baranov[35], R.J. Barlow[56], C. Barschel[40], S. Barsuk[7], W. Barter[56], F. Baryshnikov[32], V. Batozskaya[29], V. Battista[41], A. Bay[41], J. Beddow[53], F. Bedeschi[24], I. Bediaga[1], A. Beiter[61], L.J. Bel[43], N. Beliy[63], V. Bellee[41], N. Belloli[21,i], K. Belous[37], I. Belyaev[32,40], E. Ben-Haim[8], G. Bencivenni[19], S. Benson[43], S. Beranek[9], A. Berezhnoy[33], R. Bernet[42], D. Berninghoff[12], E. Bertholet[8], A. Bertolin[23], C. Betancourt[42], F. Betti[15], M.O. Bettler[40], M. van Beuzekom[43], Ia. Bezshyiko[42], S. Bifani[47], P. Billoir[8], A. Birnkraut[10], A. Bizzeti[18,u], M. Bjørn[57], T. Blake[50], F. Blanc[41], S. Blusk[61], V. Bocci[26], T. Boettcher[58], A. Bondar[36,w], N. Bondar[31], I. Bordyuzhin[32], S. Borghi[56,40], M. Borisyak[35], M. Borsato[39], F. Bossu[7], M. Boubdir[9], T.J.V. Bowcock[54], E. Bowen[42], C. Bozzi[17,40], S. Braun[12], J. Brodzicka[27], D. Brundu[16], E. Buchanan[48], C. Burr[56], A. Bursche[16,f], J. Buytaert[40], W. Byczynski[40], S. Cadeddu[16], H. Cai[64], R. Calabrese[17,g], R. Calladine[47], M. Calvi[21,i], M. Calvo Gomez[38,m], A. Camboni[38,m], P. Campana[19], D.H. Campora Perez[40], L. Capriotti[56], A. Carbone[15,e], G. Carboni[25,j], R. Cardinale[20,h], A. Cardini[16], P. Carniti[21,i], L. Carson[52], K. Carvalho Akiba[2], G. Casse[54], L. Cassina[21], M. Cattaneo[40], G. Cavallero[20,40,h], R. Cenci[24,t], D. Chamont[7], M.G. Chapman[48], M. Charles[8], Ph. Charpentier[40], G. Chatzikonstantinidis[47], M. Chefdeville[4], S. Chen[16], S.F. Cheung[57], S.-G. Chitic[40], V. Chobanova[39], M. Chrzaszcz[42], A. Chubykin[31], P. Ciambrone[19], X. Cid Vidal[39], G. Ciezarek[40], P.E.L. Clarke[52], M. Clemencic[40], H.V. Cliff[49], J. Closier[40], V. Coco[40], J. Cogan[6], E. Cogneras[5], V. Cogoni[16,f], L. Cojocariu[30], P. Collins[40], T. Colombo[40], A. Comerma-Montells[12], A. Contu[16], G. Coombs[40], S. Coquereau[38], G. Corti[40], M. Corvo[17,g], C.M. Costa Sobral[50], B. Couturier[40], G.A. Cowan[52], D.C. Craik[58], A. Crocombe[50], M. Cruz Torres[1], R. Currie[52], C. D'Ambrosio[40], F. Da Cunha Marinho[2], C.L. Da Silva[73], E. Dall'Occo[43], J. Dalseno[48], A. Davis[3], O. De Aguiar Francisco[40], K. De Bruyn[40], S. De Capua[56], M. De Cian[12], J.M. De Miranda[1], L. De Paula[2], M. De Serio[14,d], P. De Simone[19], C.T. Dean[53], D. Decamp[4], L. Del Buono[8], B. Delaney[49], H.-P. Dembinski[11], M. Demmer[10], A. Dendek[28], D. Derkach[35], O. Deschamps[5], F. Dettori[54], B. Dey[65], A. Di Canto[40], P. Di Nezza[19], H. Dijkstra[40], F. Dordei[40], M. Dorigo[40], A. Dosil Suárez[39], L. Douglas[53], A. Dovbnya[45], K. Dreimanis[54], L. Dufour[43], G. Dujany[8], P. Durante[40], J.M. Durham[73], D. Dutta[56], R. Dzhelyadin[37], M. Dziewiecki[12], A. Dziurda[40], A. Dzyuba[31], S. Easo[51], U. Egede[55], V. Egorychev[32], S. Eidelman[36,w], S. Eisenhardt[52], U. Eitschberger[10], R. Ekelhof[10], L. Eklund[53], S. Ely[61], A. Ene[30], S. Esen[12], H.M. Evans[49], T. Evans[57], A. Falabella[15], N. Farley[47], S. Farry[54], D. Fazzini[21,i], L. Federici[25], G. Fernandez[38], P. Fernandez Declara[40], A. Fernandez Prieto[39], F. Ferrari[15], L. Ferreira Lopes[41], F. Ferreira Rodrigues[2], M. Ferro-Luzzi[40], S. Filippov[34], R.A. Fini[14], M. Fiorini[17,g], M. Firlej[28], C. Fitzpatrick[41], T. Fiutowski[28], F. Fleuret[7,b], M. Fontana[16,40], F. Fontanelli[20,h], R. Forty[40], V. Franco Lima[54], M. Frank[40], C. Frei[40], J. Fu[22,q], W. Funk[40], E. Furfaro[25,j], C. Färber[40], E. Gabriel[52], A. Gallas Torreira[39], D. Galli[15,e], S. Gallorini[23], S. Gambetta[52], M. Gandelman[2], P. Gandini[22], Y. Gao[3], L.M. Garcia Martin[71], J. García Pardiñas[39], J. Garra Tico[49], L. Garrido[38], D. Gascon[38], C. Gaspar[40], L. Gavardi[10], G. Gazzoni[5], D. Gerick[12], E. Gersabeck[56], M. Gersabeck[56], T. Gershon[50], Ph. Ghez[4], S. Gianì[41], V. Gibson[49], O.G. Girard[41], L. Giubega[30], K. Gizdov[52], V.V. Gligorov[8], D. Golubkov[32], A. Golutvin[55,69], A. Gomes[1,a], I.V. Gorelov[33], C. Gotti[21,i], E. Govorkova[43], J.P. Grabowski[12],

JHEP08(2018)174

R. Graciani Diaz[38], L.A. Granado Cardoso[40], E. Graugés[38], E. Graverini[42], G. Graziani[18], A. Grecu[30], R. Greim[9], P. Griffith[16], L. Grillo[56], L. Gruber[40], B.R. Gruberg Cazon[57], O. Grünberg[67], E. Gushchin[34], Yu. Guz[37], T. Gys[40], C. Göbel[62], T. Hadavizadeh[57], C. Hadjivasiliou[5], G. Haefeli[41], C. Haen[40], S.C. Haines[49], B. Hamilton[60], X. Han[12], T.H. Hancock[57], S. Hansmann-Menzemer[12], N. Harnew[57], S.T. Harnew[48], C. Hasse[40], M. Hatch[40], J. He[63], M. Hecker[55], K. Heinicke[10], A. Heister[9], K. Hennessy[54], P. Henrard[5], L. Henry[71], E. van Herwijnen[40], M. Heß[67], A. Hicheur[2], D. Hill[57], P.H. Hopchev[41], W. Hu[65], W. Huang[63], Z.C. Huard[59], W. Hulsbergen[43], T. Humair[55], M. Hushchyn[35], D. Hutchcroft[54], P. Ibis[10], M. Idzik[28], P. Ilten[47], R. Jacobsson[40], J. Jalocha[57], E. Jans[43], A. Jawahery[60], F. Jiang[3], M. John[57], D. Johnson[40], C.R. Jones[49], C. Joram[40], B. Jost[40], N. Jurik[57], S. Kandybei[45], M. Karacson[40], J.M. Kariuki[48], S. Karodia[53], N. Kazeev[35], M. Kecke[12], F. Keizer[49], M. Kelsey[61], M. Kenzie[49], T. Ketel[44], E. Khairullin[35], B. Khanji[12], C. Khurewathanakul[41], K.E. Kim[61], T. Kirn[9], S. Klaver[19], K. Klimaszewski[29], T. Klimkovich[11], S. Koliiev[46], M. Kolpin[12], R. Kopecna[12], P. Koppenburg[43], A. Kosmyntseva[32], S. Kotriakhova[31], M. Kozeiha[5], L. Kravchuk[34], M. Kreps[50], F. Kress[55], P. Krokovny[36,w], W. Krzemien[29], W. Kucewicz[27,l], M. Kucharczyk[27], V. Kudryavtsev[36,w], A.K. Kuonen[41], T. Kvaratskheliya[32,40], D. Lacarrere[40], G. Lafferty[56], A. Lai[16], G. Lanfranchi[19], C. Langenbruch[9], T. Latham[50], C. Lazzeroni[47], R. Le Gac[6], A. Leflat[33,40], J. Lefrançois[7], R. Lefèvre[5], F. Lemaitre[40], E. Lemos Cid[39], P. Lenisa[17], O. Leroy[6], T. Lesiak[27], B. Leverington[12], P.-R. Li[63], T. Li[3], Y. Li[7], Z. Li[61], X. Liang[61], T. Likhomanenko[68], R. Lindner[40], F. Lionetto[42], V. Lisovskyi[7], X. Liu[3], D. Loh[50], A. Loi[16], I. Longstaff[53], J.H. Lopes[2], D. Lucchesi[23,o], M. Lucio Martinez[39], A. Lupato[23], E. Luppi[17,g], O. Lupton[40], A. Lusiani[24], X. Lyu[63], F. Machefert[7], F. Maciuc[30], V. Macko[41], P. Mackowiak[10], S. Maddrell-Mander[48], O. Maev[31,40], K. Maguire[56], D. Maisuzenko[31], M.W. Majewski[28], S. Malde[57], B. Malecki[27], A. Malinin[68], T. Maltsev[36,w], G. Manca[16,f], G. Mancinelli[6], D. Marangotto[22,q], J. Maratas[5,v], J.F. Marchand[4], U. Marconi[15], C. Marin Benito[38], M. Marinangeli[41], P. Marino[41], J. Marks[12], G. Martellotti[26], M. Martin[6], M. Martinelli[41], D. Martinez Santos[39], F. Martinez Vidal[71], A. Massafferri[1], R. Matev[40], A. Mathad[50], Z. Mathe[40], C. Matteuzzi[21], A. Mauri[42], E. Maurice[7,b], B. Maurin[41], A. Mazurov[47], M. McCann[55,40], A. McNab[56], R. McNulty[13], J.V. Mead[54], B. Meadows[59], C. Meaux[6], F. Meier[10], N. Meinert[67], D. Melnychuk[29], M. Merk[43], A. Merli[22,40,q], E. Michielin[23], D.A. Milanes[66], E. Millard[50], M.-N. Minard[4], L. Minzoni[17], D.S. Mitzel[12], A. Mogini[8], J. Molina Rodriguez[1], T. Mombächer[10], I.A. Monroy[66], S. Monteil[5], M. Morandin[23], M.J. Morello[24,t], O. Morgunova[68], J. Moron[28], A.B. Morris[52], R. Mountain[61], F. Muheim[52], M. Mulder[43], D. Müller[40], J. Müller[10], K. Müller[42], V. Müller[10], P. Naik[48], T. Nakada[41], R. Nandakumar[51], A. Nandi[57], I. Nasteva[2], M. Needham[52], N. Neri[22,40], S. Neubert[12], N. Neufeld[40], M. Neuner[12], T.D. Nguyen[41], C. Nguyen-Mau[41,n], S. Nieswand[9], R. Niet[10], N. Nikitin[33], T. Nikodem[12], A. Nogay[68], D.P. O'Hanlon[50], A. Oblakowska-Mucha[28], V. Obraztsov[37], S. Ogilvy[19], R. Oldeman[16,f], C.J.G. Onderwater[72], A. Ossowska[27], J.M. Otalora Goicochea[2], P. Owen[42], A. Oyanguren[71], P.R. Pais[41], A. Palano[14], M. Palutan[19,40], G. Panshin[70], A. Papanestis[51], M. Pappagallo[52], L.L. Pappalardo[17,g], W. Parker[60], C. Parkes[56], G. Passaleva[18,40], A. Pastore[14], M. Patel[55], C. Patrignani[15,e], A. Pearce[40], A. Pellegrino[43], G. Penso[26], M. Pepe Altarelli[40], S. Perazzini[40], D. Pereima[32], P. Perret[5], L. Pescatore[41], K. Petridis[48], A. Petrolini[20,h], A. Petrov[68], M. Petruzzo[22,q], E. Picatoste Olloqui[38], B. Pietrzyk[4], G. Pietrzyk[41], M. Pikies[27], D. Pinci[26], F. Pisani[40], A. Pistone[20,h], A. Piucci[12], V. Placinta[30], S. Playfer[52], M. Plo Casasus[39], F. Polci[8], M. Poli Lener[19], A. Poluektov[50], I. Polyakov[61], E. Polycarpo[2], G.J. Pomery[48], S. Ponce[40], A. Popov[37], D. Popov[11,40], S. Poslavskii[37], C. Potterat[2], E. Price[48], J. Prisciandaro[39], C. Prouve[48], V. Pugatch[46], A. Puig Navarro[42], H. Pullen[57], G. Punzi[24,p], W. Qian[50], J. Qin[63], R. Quagliani[8], B. Quintana[5], B. Rachwal[28], J.H. Rademacker[48], M. Rama[24], M. Ramos Pernas[39],

JHEP08(2018)174

M.S. Rangel[2], I. Raniuk[45,†], F. Ratnikov[35,x], G. Raven[44], M. Ravonel Salzgeber[40], M. Reboud[4], F. Redi[41], S. Reichert[10], A.C. dos Reis[1], C. Remon Alepuz[71], V. Renaudin[7], S. Ricciardi[51], S. Richards[48], M. Rihl[40], K. Rinnert[54], P. Robbe[7], A. Robert[8], A.B. Rodrigues[41], E. Rodrigues[59], J.A. Rodriguez Lopez[66], A. Rogozhnikov[35], S. Roiser[40], A. Rollings[57], V. Romanovskiy[37], A. Romero Vidal[39,40], M. Rotondo[19], M.S. Rudolph[61], T. Ruf[40], P. Ruiz Valls[71], J. Ruiz Vidal[71], J.J. Saborido Silva[39], E. Sadykhov[32], N. Sagidova[31], B. Saitta[16,f], V. Salustino Guimaraes[62], C. Sanchez Mayordomo[71], B. Sanmartin Sedes[39], R. Santacesaria[26], C. Santamarina Rios[39], M. Santimaria[19], E. Santovetti[25,j], G. Sarpis[56], A. Sarti[19,k], C. Satriano[26,s], A. Satta[25], D.M. Saunders[48], D. Savrina[32,33], S. Schael[9], M. Schellenberg[10], M. Schiller[53], H. Schindler[40], M. Schmelling[11], T. Schmelzer[10], B. Schmidt[40], O. Schneider[41], A. Schopper[40], H.F. Schreiner[59], M. Schubiger[41], M.H. Schune[7], R. Schwemmer[40], B. Sciascia[19], A. Sciubba[26,k], A. Semennikov[32], E.S. Sepulveda[8], A. Sergi[47], N. Serra[42], J. Serrano[6], L. Sestini[23], P. Seyfert[40], M. Shapkin[37], Y. Shcheglov[31,†], T. Shears[54], L. Shekhtman[36,w], V. Shevchenko[68], B.G. Siddi[17], R. Silva Coutinho[42], L. Silva de Oliveira[2], G. Simi[23,o], S. Simone[14,d], N. Skidmore[48], T. Skwarnicki[61], I.T. Smith[52], J. Smith[49], M. Smith[55], l. Soares Lavra[1], M.D. Sokoloff[59], F.J.P. Soler[53], B. Souza De Paula[2], B. Spaan[10], P. Spradlin[53], F. Stagni[40], M. Stahl[12], S. Stahl[40], P. Stefko[41], S. Stefkova[55], O. Steinkamp[42], S. Stemmle[12], O. Stenyakin[37], M. Stepanova[31], H. Stevens[10], S. Stone[61], B. Storaci[42], S. Stracka[24,p], M.E. Stramaglia[41], M. Straticiuc[30], U. Straumann[42], S. Strokov[70], J. Sun[3], L. Sun[64], K. Swientek[28], V. Syropoulos[44], T. Szumlak[28], M. Szymanski[63], S. T'Jampens[4], A. Tayduganov[6], T. Tekampe[10], G. Tellarini[17,g], F. Teubert[40], E. Thomas[40], J. van Tilburg[43], M.J. Tilley[55], V. Tisserand[5], M. Tobin[41], S. Tolk[49], L. Tomassetti[17,g], D. Tonelli[24], R. Tourinho Jadallah Aoude[1], E. Tournefier[4], M. Traill[53], M.T. Tran[41], M. Tresch[42], A. Trisovic[49], A. Tsaregorodtsev[6], P. Tsopelas[43], A. Tully[49], N. Tuning[43,40], A. Ukleja[29], A. Usachov[7], A. Ustyuzhanin[35], U. Uwer[12], C. Vacca[16,f], A. Vagner[70], V. Vagnoni[15,40], A. Valassi[40], S. Valat[40], G. Valenti[15], R. Vazquez Gomez[40], P. Vazquez Regueiro[39], S. Vecchi[17], M. van Veghel[43], J.J. Velthuis[48], M. Veltri[18,r], G. Veneziano[57], A. Venkateswaran[61], T.A. Verlage[9], M. Vernet[5], M. Vesterinen[57], J.V. Viana Barbosa[40], D. Vieira[63], M. Vieites Diaz[39], H. Viemann[67], X. Vilasis-Cardona[38,m], A. Vitkovskiy[43], M. Vitti[49], V. Volkov[33], A. Vollhardt[42], B. Voneki[40], A. Vorobyev[31], V. Vorobyev[36,w], C. Voß[9], J.A. de Vries[43], C. Vázquez Sierra[43], R. Waldi[67], J. Walsh[24], J. Wang[61], Y. Wang[65], D.R. Ward[49], H.M. Wark[54], N.K. Watson[47], D. Websdale[55], A. Weiden[42], C. Weisser[58], M. Whitehead[40], J. Wicht[50], G. Wilkinson[57], M. Wilkinson[61], M.R.J. Williams[56], M. Williams[58], T. Williams[47], F.F. Wilson[51,40], J. Wimberley[60], M. Winn[7], J. Wishahi[10], W. Wislicki[29], M. Witek[27], G. Wormser[7], S.A. Wotton[49], K. Wyllie[40], Y. Xie[65], M. Xu[65], Q. Xu[63], Z. Xu[3], Z. Xu[4], Z. Yang[3], Z. Yang[60], Y. Yao[61], H. Yin[65], J. Yu[65], X. Yuan[61], O. Yushchenko[37], K.A. Zarebski[47], M. Zavertyaev[11,c], L. Zhang[3], Y. Zhang[7], A. Zhelezov[12], Y. Zheng[63], X. Zhu[3], V. Zhukov[9,33], J.B. Zonneveld[52], S. Zucchelli[15]

[1] *Centro Brasileiro de Pesquisas Físicas (CBPF), Rio de Janeiro, Brazil*
[2] *Universidade Federal do Rio de Janeiro (UFRJ), Rio de Janeiro, Brazil*
[3] *Center for High Energy Physics, Tsinghua University, Beijing, China*
[4] *Univ. Grenoble Alpes, Univ. Savoie Mont Blanc, CNRS, IN2P3-LAPP, Annecy, France*
[5] *Clermont Université, Université Blaise Pascal, CNRS/IN2P3, LPC, Clermont-Ferrand, France*
[6] *Aix Marseille Univ, CNRS/IN2P3, CPPM, Marseille, France*
[7] *LAL, Univ. Paris-Sud, CNRS/IN2P3, Université Paris-Saclay, Orsay, France*
[8] *LPNHE, Université Pierre et Marie Curie, Université Paris Diderot, CNRS/IN2P3, Paris, France*
[9] *I. Physikalisches Institut, RWTH Aachen University, Aachen, Germany*
[10] *Fakultät Physik, Technische Universität Dortmund, Dortmund, Germany*
[11] *Max-Planck-Institut für Kernphysik (MPIK), Heidelberg, Germany*

JHEP08(2018)174

[12] Physikalisches Institut, Ruprecht-Karls-Universität Heidelberg, Heidelberg, Germany
[13] School of Physics, University College Dublin, Dublin, Ireland
[14] Sezione INFN di Bari, Bari, Italy
[15] Sezione INFN di Bologna, Bologna, Italy
[16] Sezione INFN di Cagliari, Cagliari, Italy
[17] Universita e INFN, Ferrara, Ferrara, Italy
[18] Sezione INFN di Firenze, Firenze, Italy
[19] Laboratori Nazionali dell'INFN di Frascati, Frascati, Italy
[20] Sezione INFN di Genova, Genova, Italy
[21] Sezione INFN di Milano Bicocca, Milano, Italy
[22] Sezione di Milano, Milano, Italy
[23] Sezione INFN di Padova, Padova, Italy
[24] Sezione INFN di Pisa, Pisa, Italy
[25] Sezione INFN di Roma Tor Vergata, Roma, Italy
[26] Sezione INFN di Roma La Sapienza, Roma, Italy
[27] Henryk Niewodniczanski Institute of Nuclear Physics Polish Academy of Sciences, Kraków, Poland
[28] AGH - University of Science and Technology, Faculty of Physics and Applied Computer Science, Kraków, Poland
[29] National Center for Nuclear Research (NCBJ), Warsaw, Poland
[30] Horia Hulubei National Institute of Physics and Nuclear Engineering, Bucharest-Magurele, Romania
[31] Petersburg Nuclear Physics Institute (PNPI), Gatchina, Russia
[32] Institute of Theoretical and Experimental Physics (ITEP), Moscow, Russia
[33] Institute of Nuclear Physics, Moscow State University (SINP MSU), Moscow, Russia
[34] Institute for Nuclear Research of the Russian Academy of Sciences (INR RAS), Moscow, Russia
[35] Yandex School of Data Analysis, Moscow, Russia
[36] Budker Institute of Nuclear Physics (SB RAS), Novosibirsk, Russia
[37] Institute for High Energy Physics (IHEP), Protvino, Russia
[38] ICCUB, Universitat de Barcelona, Barcelona, Spain
[39] Instituto Galego de Física de Altas Enerxías (IGFAE), Universidade de Santiago de Compostela, Santiago de Compostela, Spain
[40] European Organization for Nuclear Research (CERN), Geneva, Switzerland
[41] Institute of Physics, Ecole Polytechnique Fédérale de Lausanne (EPFL), Lausanne, Switzerland
[42] Physik-Institut, Universität Zürich, Zürich, Switzerland
[43] Nikhef National Institute for Subatomic Physics, Amsterdam, The Netherlands
[44] Nikhef National Institute for Subatomic Physics and VU University Amsterdam, Amsterdam, The Netherlands
[45] NSC Kharkiv Institute of Physics and Technology (NSC KIPT), Kharkiv, Ukraine
[46] Institute for Nuclear Research of the National Academy of Sciences (KINR), Kyiv, Ukraine
[47] University of Birmingham, Birmingham, United Kingdom
[48] H.H. Wills Physics Laboratory, University of Bristol, Bristol, United Kingdom
[49] Cavendish Laboratory, University of Cambridge, Cambridge, United Kingdom
[50] Department of Physics, University of Warwick, Coventry, United Kingdom
[51] STFC Rutherford Appleton Laboratory, Didcot, United Kingdom
[52] School of Physics and Astronomy, University of Edinburgh, Edinburgh, United Kingdom
[53] School of Physics and Astronomy, University of Glasgow, Glasgow, United Kingdom
[54] Oliver Lodge Laboratory, University of Liverpool, Liverpool, United Kingdom
[55] Imperial College London, London, United Kingdom
[56] School of Physics and Astronomy, University of Manchester, Manchester, United Kingdom
[57] Department of Physics, University of Oxford, Oxford, United Kingdom
[58] Massachusetts Institute of Technology, Cambridge, MA, United States
[59] University of Cincinnati, Cincinnati, OH, United States

JHEP08(2018)174

[60] University of Maryland, College Park, MD, United States
[61] Syracuse University, Syracuse, NY, United States
[62] Pontifícia Universidade Católica do Rio de Janeiro (PUC-Rio), Rio de Janeiro, Brazil, associated to [2]
[63] University of Chinese Academy of Sciences, Beijing, China, associated to [3]
[64] School of Physics and Technology, Wuhan University, Wuhan, China, associated to [3]
[65] Institute of Particle Physics, Central China Normal University, Wuhan, Hubei, China, associated to [3]
[66] Departamento de Fisica, Universidad Nacional de Colombia, Bogota, Colombia, associated to [8]
[67] Institut für Physik, Universität Rostock, Rostock, Germany, associated to [12]
[68] National Research Centre Kurchatov Institute, Moscow, Russia, associated to [32]
[69] National University of Science and Technology MISIS, Moscow, Russia, associated to [32]
[70] National Research Tomsk Polytechnic University, Tomsk, Russia, associated to [32]
[71] Instituto de Fisica Corpuscular, Centro Mixto Universidad de Valencia - CSIC, Valencia, Spain, associated to [38]
[72] Van Swinderen Institute, University of Groningen, Groningen, The Netherlands, associated to [43]
[73] Los Alamos National Laboratory (LANL), Los Alamos, United States, associated to [61]

[a] Universidade Federal do Triângulo Mineiro (UFTM), Uberaba-MG, Brazil
[b] Laboratoire Leprince-Ringuet, Palaiseau, France
[c] P.N. Lebedev Physical Institute, Russian Academy of Science (LPI RAS), Moscow, Russia
[d] Università di Bari, Bari, Italy
[e] Università di Bologna, Bologna, Italy
[f] Università di Cagliari, Cagliari, Italy
[g] Università di Ferrara, Ferrara, Italy
[h] Università di Genova, Genova, Italy
[i] Università di Milano Bicocca, Milano, Italy
[j] Università di Roma Tor Vergata, Roma, Italy
[k] Università di Roma La Sapienza, Roma, Italy
[l] AGH - University of Science and Technology, Faculty of Computer Science, Electronics and Telecommunications, Kraków, Poland
[m] LIFAELS, La Salle, Universitat Ramon Llull, Barcelona, Spain
[n] Hanoi University of Science, Hanoi, Vietnam
[o] Università di Padova, Padova, Italy
[p] Università di Pisa, Pisa, Italy
[q] Università degli Studi di Milano, Milano, Italy
[r] Università di Urbino, Urbino, Italy
[s] Università della Basilicata, Potenza, Italy
[t] Scuola Normale Superiore, Pisa, Italy
[u] Università di Modena e Reggio Emilia, Modena, Italy
[v] Iligan Institute of Technology (IIT), Iligan, Philippines
[w] Novosibirsk State University, Novosibirsk, Russia
[x] National Research University Higher School of Economics, Moscow, Russia
[†] Deceased

JHEP08(2018)174